# Numerical study of photonic crystals with a split band edge: Polarization dependence and sensitivity analysis

K.-Y. Jung* and F. L. Teixeira
*ElectroScience Laboratory and Department of Electrical and Computer Engineering, The Ohio State University, 1320 Kinnear Road, Columbus, Ohio 43212, USA*

(Received 6 August 2008; published 29 October 2008)

We examine photonic crystals (PhC) made of periodic stacks of anisotropic dielectric layers with a split band edge (SBE) on the band diagram. Just below the band edge frequency, the dispersion relation $\omega(k)$ of SBE PhCs can be approximated as a linear combination of a quadratic term and a quartic term. This is in contrast to regular (conventional) band edge PhCs, which produce a quadratic dispersion relation, and to degenerate band edge (DBE) PhCs, which produce a quartic dispersion relation. Finite-size DBE PhCs and SBE PhCs are of interest because they both can support slow-wave Fabry-Perot resonances with very good transmittance. One of the most significant differences between DBE and SBE is that the transmittance of the former depends on the incident wave polarization whereas in the latter it does not. In this work, we investigate the transmittance behavior of SBE PhCs and perform a sensitivity analysis of their responses against geometrical and/or material perturbations. Dielectric losses, thickness perturbations, and misalignment angle perturbations are considered. The analysis uses a full-wave numerical technique for transient Maxwell's equations in inhomogeneous anisotropic media based on a complex-envelope alternating-direction-implicit finite-difference time-domain. A comparison is also made between the sensitivity of the SBE PhCs response versus that of DBE PhCs.

DOI: 10.1103/PhysRevA.78.043826 PACS number(s): 42.70.Qs, 42.25.Bs, 41.20.Jb

## I. INTRODUCTION

Periodic metamaterials in which the dispersion relation $\omega(k)$ can be tailored by a judicious choice of geometry and constitutive parameters [1–11] have great potential for applications at rf, microwave, and optical frequency ranges [12–17]. For example, one-dimensional photonic crystals (PhCs) with unit cells composed of ferromagnetic materials and misaligned anisotropic dielectric layers can yield an asymmetric dispersion diagram with a stationary inflection point (SIP) [2]. At the SIP frequency, electromagnetic waves propagate with a vanishing group velocity, leading to frozen modes and gigantic field intensity enhancement [2,6,17]. Similarly, PhCs made up of one isotropic layer and two misaligned anisotropic dielectric layers in each period can yield a degenerate band edge (DBE) [4,5,8,10] on the band diagram with a quartic (hence, flatter) dispersion relation just below the band-edge frequency $\omega_{BE}$. Finite-size DBE PhCs also yield good transmittance and a dramatic increase in the field intensity due to a different reason: the interplay of vanishing group velocity near $\omega_{BE}$ and good transmittance at the Fabry-Perot resonances close to it.

The transmittance of DBE PhCs, however, depends on the polarization of the incident wave. DBE PhCs support a reciprocal pair of propagating Bloch modes and a reciprocal pair of evanescent Bloch modes in vicinity of $\omega_{BE}$. Therefore, only one (elliptical) polarization component of incident waves is matched to propagating (real wave number) modes and well coupled into the DBE PhCs. The other (elliptical) polarization component is only matched to evanescent (imaginary wave number) modes and reflected back. To circumvent this problem while maintaining slow-wave Fabry-Perot resonances, new dispersion-engineered periodic stacks—refereed to as split band edge (SBE) PhCs—have been recently proposed [11]. The unit cell of SBE PhCs can be configured in the same fashion as that of DBE PhCs, viz. one isotropic layer and two misaligned anisotropic dielectric layers. The dispersion relation $\omega(k)$ in SBE PhCs is approximated by a sum of a quadratic term and a quartic term. In vicinity of the SBE frequency, all four (two reciprocal pairs) Bloch modes are propagating and thus good impedance matching (transmittance) is possible regardless of polarization of incident waves [11]. In addition, for a given number of cells, it has been shown that SBE PhCs can produce stronger resonant transmissions than DBE PhCs [18].

In this work, we examine the behavior of the transmittance and field enhancement effects in SBE PhCs as a function of the incident wave polarization and contrast it against the DBE PhC performance. In addition, we perform a sensitivity analysis of SBE PhC responses with respect to geometrical and material perturbations. Since the periodicity is broken in those cases, full-wave numerical techniques for solving Maxwell's equations in general anisotropic media are necessary. In particular, we adopt a complex-envelope (CE) alternating-direction-implicit (ADI) finite-difference time-domain (FDTD) method [9,19,20] for the analysis of SBE PhCs. We have previously demonstrated the accuracy and computational suitability of the CE-ADI-FDTD algorithm for the analysis of DBE PhCs [10]. Because rapid field variations inside DBE or SBE PhCs require highly refined grids, two characteristics of the CE-ADI-FDTD in particular make it the ideal candidate for the present full-wave analysis and allow the sensitivity analysis to become practical: (i) its unconditional stability that allows for larger time steps not bounded by the Courant limit and (ii) its very low grid-dispersion error near to the carrier frequency that allows accurate results to be obtained using Courant numbers beyond

*jung.166@osu.edu

 

100. Further details on the CE-ADI-FDTD algorithm can be found in the Appendix of Ref. [10].

The remainder of this paper is organized as follows. In Sec. II, we design a SBE PhC by modifying a DBE PhC so that the misalignment angle between two anisotropic layers is changed while other parameters remain fixed. This leads to a fair comparison of sensitivities between the SBE PhC and the DBE PhC since material and geometrical properties are similar. Numerical results comparing the performance of the SBE PhC and the performance of the DBE PhC under various incident wave polarizations are presented in Sec. III. In Sec. IV, a sensitivity analysis of SBE PhC responses against dielectric losses is carried out. In addition, the effect of layer thickness variations, misalignment angle variations, and their interplay is considered, with a further comparison against the DBE PhC also made. Concluding remarks are provided in Sec. V.

## II. DISPERSION CHARACTERISTICS OF SBE PHOTONIC CRYSTALS

Just below $\omega_{\mathrm{BE}}$, the dispersion curve of the SBE is approximated as [11]

$$\nu_{\mathrm{SBE}}(\kappa) \approx \frac{a}{2}\kappa^2 + \frac{b}{4}\kappa^4 \tag{1}$$

with $\kappa = |k - k_0|L$ and $\nu(\kappa) = [\omega(k) - \omega(k_0)]L/c_0$, where $k_0$ indicates a stationary point (i.e., 0 or $\pi/L$), $k$ is the Bloch wave number, $\omega$ is the angular frequency, $L$ is the unit cell length, and $c_0$ is speed of light in vacuum. On the other hand, for regular band edge (RBE) and DBE PhCs we have $\nu_{\mathrm{RBE}}(\kappa) \approx \frac{a}{2}\kappa^2$ and $\nu_{\mathrm{DBE}}(\kappa) \approx \frac{b}{4}\kappa^4$, respectively.

A key condition for SBE behavior is

$$a/b < 0 \tag{2}$$

so that its dispersion curve has both concave and convex regions. In addition, the dispersion curve should satisfy the following (proximity) condition:

$$|a/b| \ll 1. \tag{3}$$

The above is required for gigantic field intensity enhancement as present in DBE PhCs ($a=0$).

We consider periodic stacks composed of three layers in the unit cell: one anisotropic layer ($A1$ layer), one isotropic layer ($B$ layer), and a second anisotropic layer ($A2$ layer), in this sequence. For simplicity, we assume that the $B$ layer is air. The dispersion relation can be tailored in order to support the SBE or the DBE by adjusting geometrical and material properties in the unit cell. The permittivity tensor of the $A$ layers with anisotropy in the $xy$ plane can be expressed as

$$[\epsilon_A] = \epsilon_0 \begin{bmatrix} \epsilon_A + \delta_A \cos(2\phi_A) & \delta_A \sin(2\phi_A) & 0 \\ \delta_A \sin(2\phi_A) & \epsilon_A - \delta_A \cos(2\phi_A) & 0 \\ 0 & 0 & \epsilon_{zz} \end{bmatrix}, \tag{4}$$

where $\delta_A$ is the magnitude of in-plane anisotropy and $\phi_A$ is the orientation angle of the principal axis of the permittivity tensor in the $xy$ plane. For the design of a SBE PhC, we modify the DBE PhC considered in Ref. [10]. The constitutive tensor (relative) parameters of the DBE PhC are $\epsilon_{A1} = \epsilon_{A2} = 13.61$; $\delta_{A1} = \delta_{A2} = 12.4$; $\phi_{A1} = 0°$, $\phi_{A2} = 45°$; $\mu_{r,A1} = \mu_{r,A2} = 1$. The layer thicknesses are $L_{A1} = L_{A2} = 0.270545$ m and $L_B = 0.45891$ m.

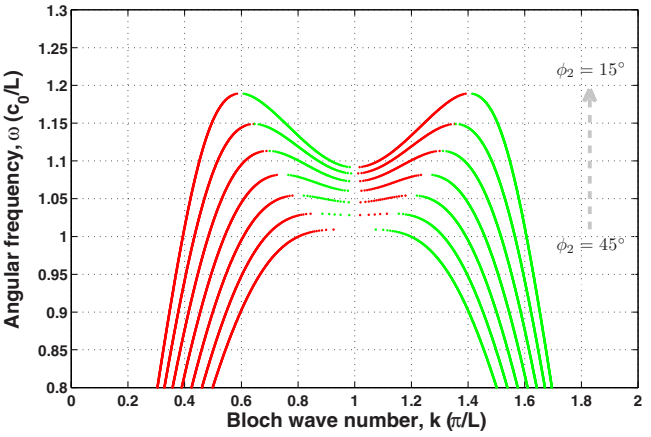


FIG. 1. (Color online) Changes in the dispersion curve $\omega(k)$ by adjusting in the misalignment angle $\phi_{A2}$ of $A_2$ layer. By decreasing $\phi_{A2}$ from $\phi_{A2} = 45°$, the DBE PhC configuration is changed to a SBE PhC configuration.

We modify the above PhC by changing $\phi_{A2}$ while keeping the other parameters fixed [21]. As shown in Fig. 1, a decrease in $\phi_{A2}$ develops a SBE in the dispersion curve [22]. We consider two cases: $\phi_{A2} = 15°$ and $\phi_{A2} = 35°$. The dispersion curves of these cases can be fitted to the relation in Eq. (1). From a curve fit, we have $a = 0.2486$ and $b = -0.1635$ for the former and $a = 0.0899$ and $b = -0.2163$ for the latter. Although both PhCs satisfy the condition in Eq. (2), the latter satisfies the DBE proximity condition in Eq. (3), but the former does not. Hence, we consider $\phi_{A2} = 35°$ in what follows. We note that there is a tradeoff between the DBE proximity condition and the SBE frequency range (i.e., the frequency range in which all four Bloch modes propagate). As a dispersion curve deviates from the DBE (in this study: as $\phi_{A2}$ decreases), it yields a wider SBE frequency range but with more deviation from the proximity condition.

In general, the impedance mismatch is worsened as the frequency of operation approaches $\omega_{\mathrm{BE}}$ for a semi-infinite periodic stack [8,10]. As mentioned before, good matching (transmittance) can be achieved by exploiting Fabry-Perot resonances associated with finite-size periodic stacks. As the number $N$ of unit cells increases, the Fabry-Perot resonance frequencies move closer to the band edge frequency and thus electromagnetic waves can propagate extremely slowly inside the crystal while maintaining good transmittance [8,10]. For DBE PhCs, the choice of $N$ may be arbitrary once all other application-specific criteria (overall physical size, operating frequency, quality factor $Q$, etc.) are attained. For SBE PhCs, however, $N$ should be judiciously chosen so that SBE PhCs operate at the double SBE resonance condition, viz. the condition for two cavity resonances (associated with two reciprocal pairs of propagating Bloch modes) occurring at the same (or nearly the same) frequency, as pointed out in Ref. [11]. Numerical examples will be provided in the next section to illustrate this point.

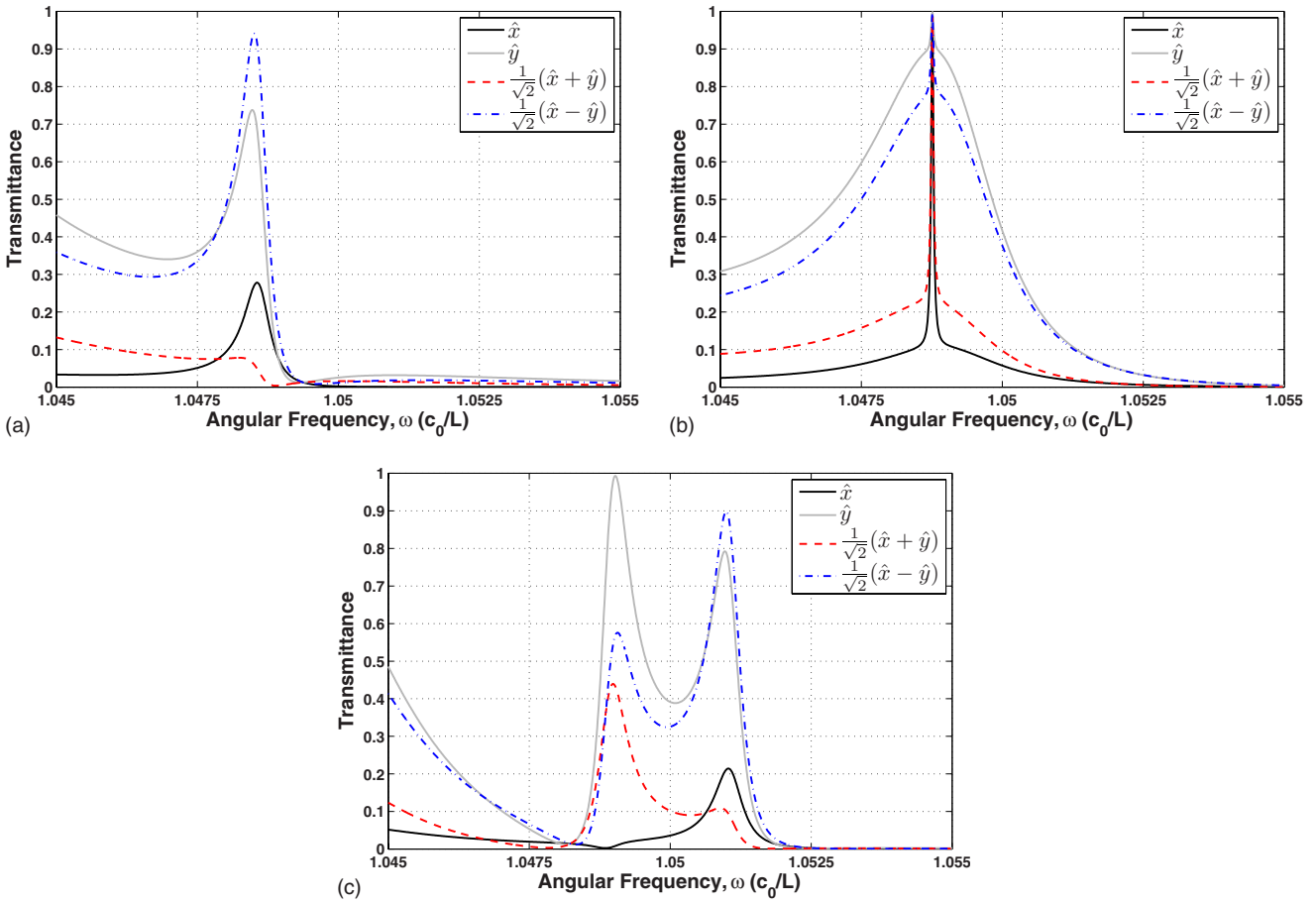


FIG. 2. (Color online) Transmittance of the SBE PhC versus the number $N$ of unit cells for different polarizations. (a) $N=9$, (b) $N=11$, (c) $N=13$. Unit transmittance (perfect impedance matching) is obtained at the Fabry-Perot cavity resonance frequency for $N=11$ regardless of the incident wave polarization. Good transmittance is obtained only in a very narrow frequency band due to the resonance behavior.

### III. POLARIZATION DEPENDENCE

We illustrate the transmittance of the SBE PhC versus $N$ under various incident wave polarizations. As shown in Fig. 2, the SBE PhC with $N=11$ leads to the polarization-independent perfect transmittance at the Fabry-Perot resonance, implying that the double SBE resonance condition is satisfied. Hence, any incident wave regardless of the polarization can be perfectly coupled into the SBE PhC with $N=11$ at the Fabry-Perot resonance. By comparison, we illustrate the effect of polarization on transmittance in the DBE PhC with $N=11$ in Fig. 3. Transmittance of the DBE PhC is highly dependent on polarization. The incident wave with $y$ polarization is mostly coupled into the DBE PhC but the incident wave with $x$ polarization is mostly reflected back. In fact, this polarization dependence exists for DBE PhCs with any $N$.

Next, we examine the field intensity inside the SBE PhC with $N=11$ at the Fabry-Perot resonance under the same polarization as considered previously. Figure 4 shows the steady-state time-averaged field intensity $|\mathbf{E}|^2$ inside the SBE PhC when the incident wave has unit amplitude. The SBE PhC produces gigantic field enhancement for all polarizations, although the magnitude of field intensity depends on the particular polarization. The field intensity distribution inside the SBE PhC results from the field due to two pairs of propagating Bloch modes. Each propagating pair is matched to each polarization but their group velocities (hence, the

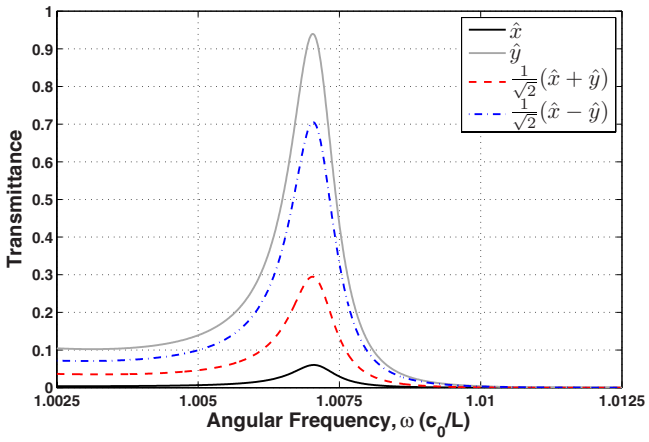


FIG. 3. (Color online) Transmittance of the DBE PhC with $N=11$ under different polarizations. The dependence of transmittance on polarization is clearly observed. This dependency is present for DBE PhCs with any $N$.

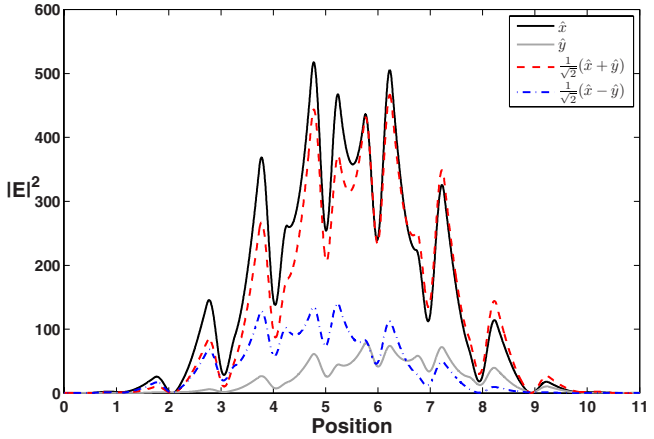


FIG. 4. (Color online) Steady-state time-averaged field intensity $|\mathbf{E}|^2$ inside the SBE PhC with $N=11$, for an incident wave with unit amplitude. Gigantic enhancement in the field intensity is visible for all polarizations, but the amount depends on the particular polarization.

field enhancement effects) are different. The relative contribution of each Bloch mode is dictated by the incident wave polarization and thus the $Q$ of the SBE PhC depends on the incident wave polarization [see Fig. 2(b)]. This explains why the field intensity depends on the polarization in spite of the polarization-independent perfect transmittance. By comparison, the DBE PhC with $N=11$ is also considered in Fig. 5. The field intensity inside the DBE PhC under $x$ polarization is very small, since a large portion of incident wave is not coupled into the PhC but reflected back. However, a dramatic increase in field intensity is observed for $y$ polarization due to good transmittance in that case.

## IV. SENSITIVITY ANALYSIS

Next, we illustrate the sensitivity of SBE PhC responses against material and geometrical perturbations. The field intensity enhancement effects under $y$ polarization are investigated and a contrast between SBE and DBE PhC responses is made. We consider four different perturbations: (i) dielectric losses, (ii) layer thickness perturbations, (iii) misalignment angle perturbations, and (iv) simultaneous perturbations on layer thickness and misalignment angle.

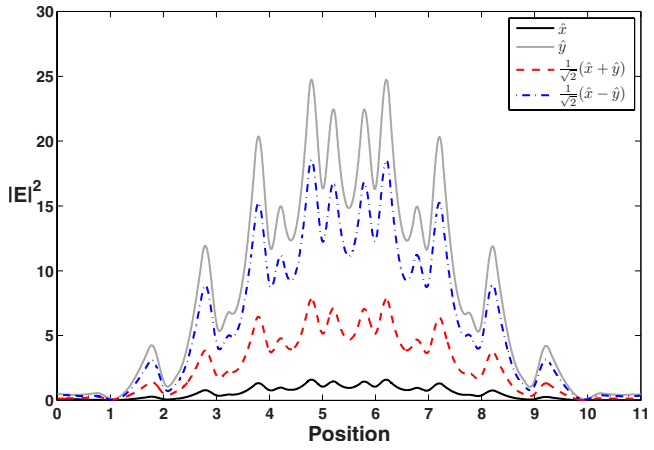


FIG. 5. (Color online) Steady-state time-averaged field intensity $|\mathbf{E}|^2$ inside the DBE PhC with $N=11$. The incident wave has unit amplitude. The incident wave with $x$ polarization is not efficiently coupled into the PhC (see Fig. 3) and thus $|\mathbf{E}|^2$ is much smaller in this case.

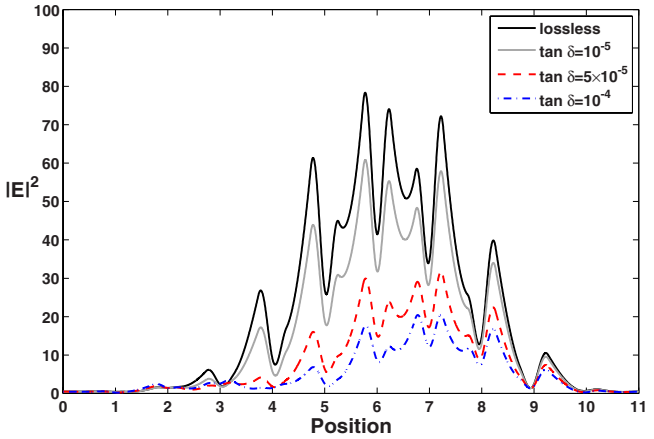


FIG. 6. (Color online) Steady-state time-averaged $|\mathbf{E}|^2$ inside the SBE PhC with dielectric losses in $A$ layers. As expected, a gradual increase in the losses leads to a monotonic decrease in the field intensity. The relative field distributions are also modified.

### A. Dielectric losses

We investigate the variation on the field intensity distribution inside the SBE PhC when dielectric losses are present in the anisotropic layers. Figure 6 and 7 show the steady-state time-averaged $|\mathbf{E}|^2$ inside the SBE PhC with $N=11$ and the DBE PhC with $N=11$, respectively. Note the order of magnitude difference in the dielectric losses considered in these two figures (see the indicated loss tangents). The effect of losses on the field intensity is more pronounced for the

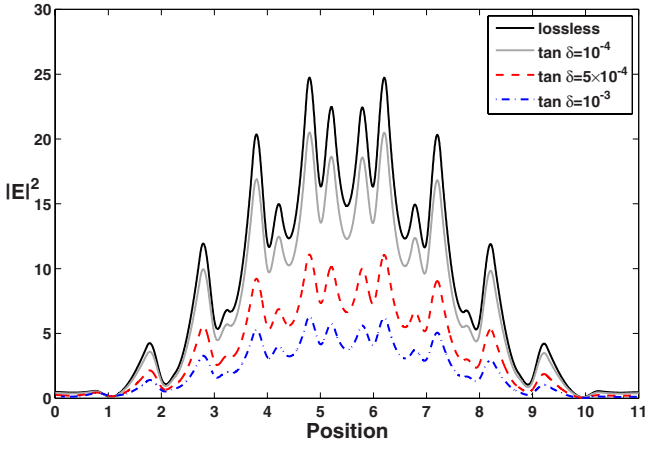


FIG. 7. (Color online) Steady-state time-averaged $|\mathbf{E}|^2$ inside the DBE PhC with dielectric losses in $A$ layers. The effect of losses is relatively less pronounced in the DBE PhC case than in the SBE PhC case. Note also that the relative field distributions are less modified compared to Fig. 6. Note the one-digit difference in the legend between Figs. 6 and 7.

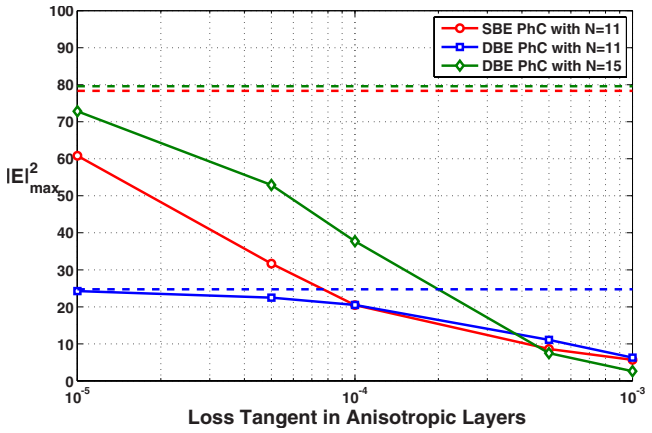


FIG. 8. (Color online) Peak value of $|\mathbf{E}|^2$ inside lossy PhCs. Lossless PhC results are also displayed by dashed lines. For same $N$, the SBE PhC is more sensitive to dielectric losses than the DBE PhC. Considering similar (field enhancement) performance, losses have stronger influence on the SBE PhC with $N=11$ than the DBE PhC with $N=15$ for low losses, but the effect is gradually reversed for higher losses.

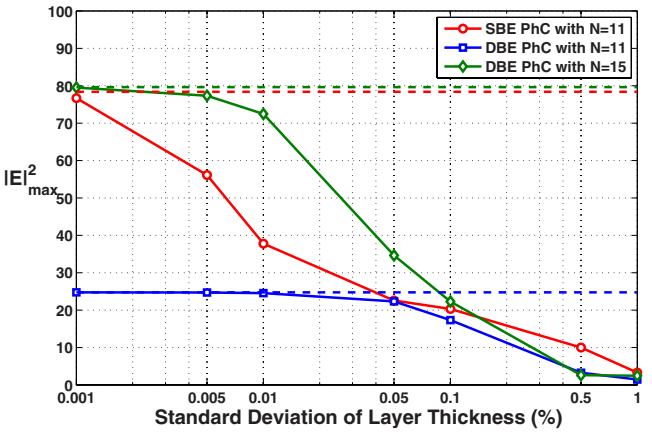


FIG. 9. (Color online) Peak value of $|\mathbf{E}|^2$ inside PhCs with all-layer thickness perturbations. The dashed lines indicate nonperturbed PhC results, for reference. Each cell thickness is assumed to be an independent Gaussian random variable with mean at the nominal thickness value. Different variances are considered. For each variance, 12 realizations are produced. The above shows the average results for each standard deviation.

SBE PhC than the DBE PhC, while the absolute intensity enhancements in the SBE PhC are still higher than in the DBE PhC when the loss tangent is below $10^{-4}$.

The relative field distribution in the SBE PhC changes as the loss tangent increases. On the other hand, the relative field distribution in the DBE PhC is mostly preserved, despite the decrease in magnitude. The change in the relative field distribution of the SBE PhC follows from the fact that the sensitivities of the two reciprocal Bloch mode pairs against dielectric losses are different. As alluded before, SBE PhC responses result from a superposition of (quadratic dispersion) RBE- and (quartic dispersion) DBE-related responses. As pointed out in Ref. [10], RBE responses are more robust than DBE responses against losses. Therefore, for SBE PhCs with higher losses, the RBE contribution becomes progressively more dominant, which alters the relative field distribution.

Figure 8 shows the peak value of $|\mathbf{E}|^2$ inside PhCs with losses. The DBE PhC with $N=15$ is also included in this case, since this DBE PhC yields field enhancement effects similar to the considered SBE PhC when lossless. Comparing the SBE PhC $N=11$ and the DBE PhC $N=15$ results, dielectric losses show stronger influence on SBE than DBE responses for low loss, but the reverse is true for high loss.

### B. Layer thickness perturbations

In this section, we examine the effect of layer thickness perturbations on PhC responses. For this purpose, we first assume the thickness of each cell to be an independent Gaussian random variable, centered on the nominal thickness. This kind of perturbation is expected from manufacturing tolerances during fabrication. The results for the peak value of $|\mathbf{E}|^2$ inside the PhCs are shown in Fig. 9. For each variance, an ensemble with 12 realizations is considered and the average result is taken. As the deviation in the layer thickness increases, the field intensity in the PhCs progressively decreases, as expected.

Next, the thickness of all cells is perturbed uniformly (systematic perturbation). This kind of perturbation is expected from calibration tolerances during fabrication. Figure 10 shows the peak value of $|\mathbf{E}|^2$ inside PhCs with perturbed layer thicknesses. It is seen that small variations in the layer thickness have a stronger impact on the SBE PhC performance than the DBE PhC performance. However, a more pronounced effect is observed on DBE than SBE for large perturbations. When the layer thickness is perturbed by 0.1%, the SBE PhC produces greater field intensity enhancement than either of the DBE PhCs considered ($N=11,15$). Field enhancement effects, however, are not observed for PhCs with above 1% error in the layer thickness because

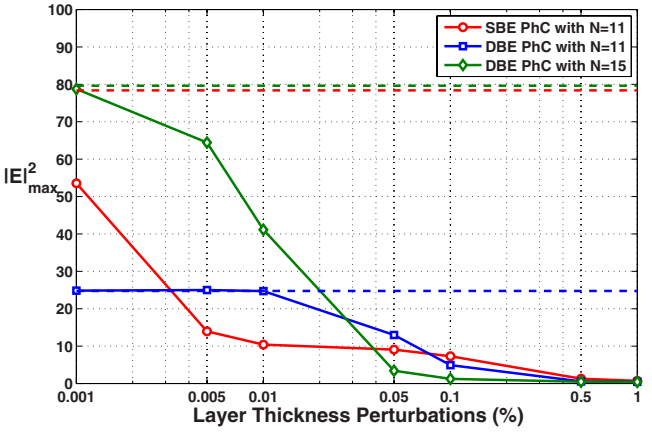


FIG. 10. (Color online) Peak value of $|\mathbf{E}|^2$ inside PhCs with all-layer thickness perturbations. In this case, the thickness of each cell is uniformly perturbed (systematic perturbation). Comparing Figs. 9 and 10, we observe that systematic perturbations have a more pronounced effect on PhC responses than Gaussian perturbations.

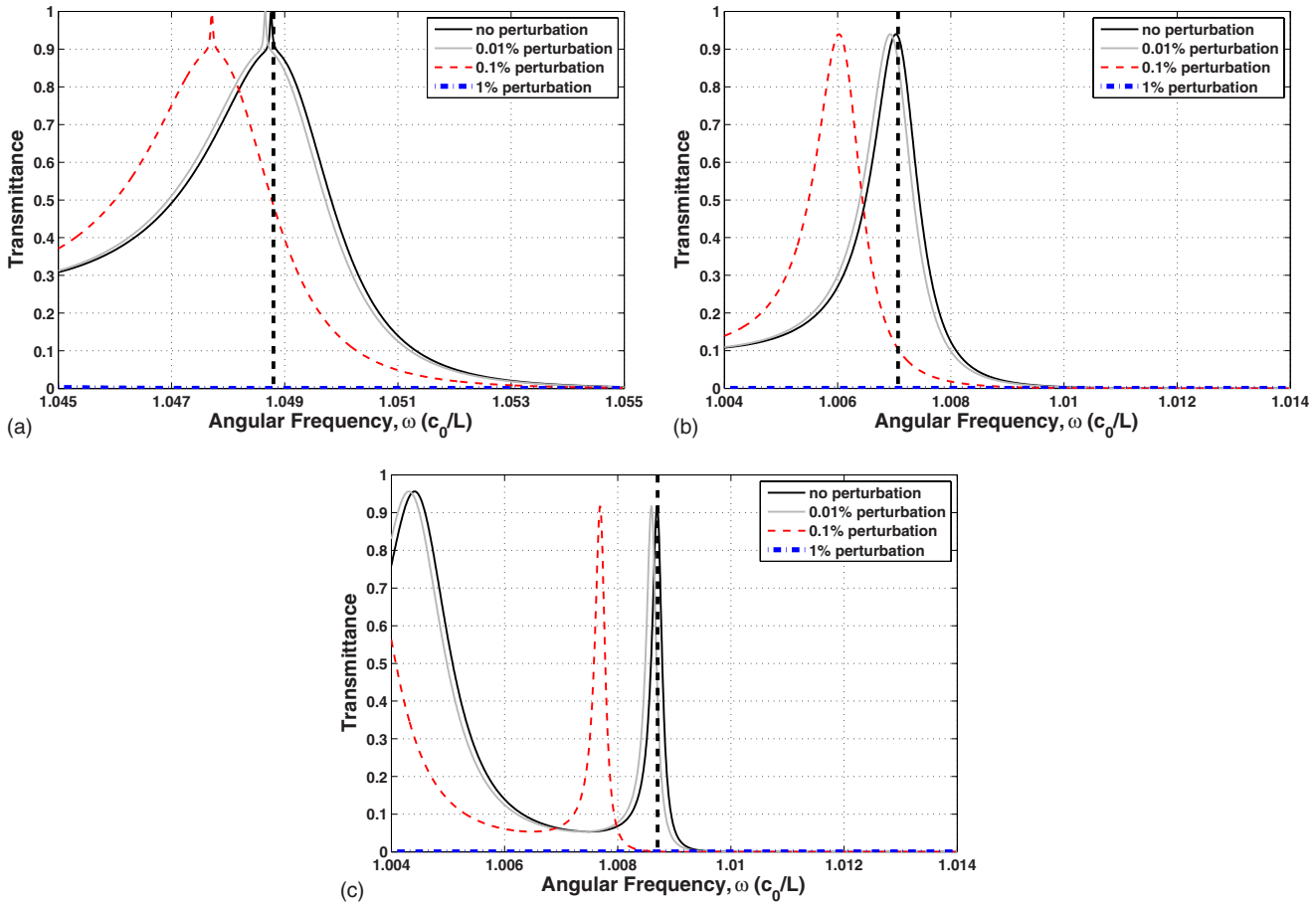


FIG. 11. (Color online) Effect of layer thickness perturbations on Fabry-Perot resonance frequency. (a) SBE PhC with $N=11$, (b) DBE PhC with $N=11$, (c) DBE PhC with $N=15$. The vertical dashed line indicates the original operating (resonance) frequency for nonperturbed PhCs. The perturbations lead to a shift of the resonance frequency and thus to a decrease in transmittance at the nominal (desired) operating frequency. Note that almost zero transmittance for all PhCs ensues with 1% thickness perturbation.

almost no incident power is coupled into the PhC in this case. Comparing Fig. 9 and Fig. 10, we also observe that systematic perturbations on the layer thickness have a more pronounced effect on PhC responses than random perturbations.

We evaluate the transmittance $\tau$ versus layer thickness perturbations in Fig. 11. As the layer thickness is perturbed, the resonance frequency is shifted to lower frequencies, leading to a poor impedance matching at the original operating frequency (resonance). From Fig. 11 we note that for 0.1% perturbation, $\tau \sim 0.5$ for the SBE PhC with $N=11$, $\tau \sim 0.1$ for the DBE PhC with $N=11$, and $\tau \sim 0$ the DBE PhC with $N=15$. For large perturbations (above 1%), however, none of the PhCs provide good matching. Hence, the enhancement in the field intensity is not observed for the 0.5% or 1% perturbations, as illustrated in Fig. 10.

### C. Misalignment angle perturbations

To illustrate the effect of orientation misalignments of the $A$ layers, we randomly perturb the orientation angles of $A$ layers. The misalignment angles are treated as independent Gaussian random variables. For each variance, an ensemble with 12 realizations is again used. Table I summarizes the peak value of $|\mathbf{E}|^2$ inside PhCs under such perturbations. We note that the SBE PhC with $N=11$ yields more field enhancement effects than DBE PhCs for the perturbations considered. For the SBE PhC with $N=11$ and the DBE PhC with $N=15$, the field intensity drops quickly under for 0.25° standard deviation in the misalignment angle but decreases more gradually under higher deviations. The DBE, $N=11$ results are considerably less sensitive to angle perturbations than the DBE, $N=15$ results.

TABLE I. Peak value of field intensity inside PhCs with misalignment angle perturbations.

| $\sqrt{V_{\mathrm{ar}}(\phi_A)}$ | SBE, $N=11$ | DBE, $N=11$ | DBE, $N=15$ |
|---|---|---|---|
| 0° | 78.38 | 24.74 | 79.60 |
| 0.25° | 17.37 | 13.40 | 10.58 |
| 0.5° | 10.36 | 8.93 | 3.26 |
| 0.75° | 8.12 | 4.49 | 2.72 |
| 1° | 5.39 | 4.09 | 2.03 |
| 2° | 4.62 | 3.30 | 1.71 |
| 3° | 2.73 | 2.25 | 1.62 |

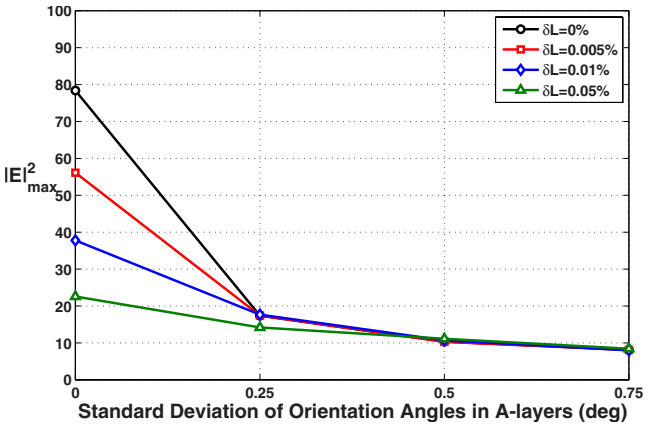


FIG. 12. (Color online) Effect of simultaneous random perturbations of layer thickness and misalignment angle on the field intensity for a SBE PhC with $N=11$. In the legend, $\delta L$ denotes the standard deviation of the layer thickness. The curve $\delta L=0$ indicates the result with misalignment angle perturbation only, as presented in Table I results.

### D. Interplay of layer thickness and misalignment angle perturbations

Finally, we assess the sensitivity of SBE PhC responses to simultaneous perturbations on the layer thickness and misalignment angle. We assume both layer thickness and misalignment angle to be an independent (each) Gaussian random variable centered on the nominal values. Figure 12 shows the peak value of $|\mathbf{E}|^2$ inside the SBE PhC with $N=11$ under thickness and misalignment angle perturbations. By comparison, we also include SBE PhC responses for misalignment angle perturbations only. For standard deviations above 0.25°, the effect of misalignment angle errors dominates the overall degradation in response, for the layer perturbations considered.

## V. CONCLUSION

We have examined the transmittance behavior and field enhancement effects in finite-size periodic stacks of anisotropic layers with SBE characteristics supporting slow-wave Fabry-Perot resonances. We have contrasted the response of PhCs with polarization-independent perfect transmittance, viz. SBE PhCs, with that of DBE PhCs. A sensitivity analysis was carried out to examine the effect of geometrical and material parameters, and the impact of these perturbations on SBE and DBE PhC responses was illustrated. In particular, we have examined the sensitivity of PhC responses to dielectric losses, layer thickness perturbations, and misalignment angle perturbations (the latter two both in isolation and combined). As expected, all above imperfections lead to a decrease in field intensity enhancement effects, for both SBE and DBE PhCs. The effect of small perturbations is in general more pronounced for SBE PhCs than for DBE PhCs, while the opposite is true for larger perturbations. For the perturbation ranges considered, it has been observed that the SBE PhC responses are more sensitive to misalignment angle perturbations than layer thickness perturbations when those are considered simultaneously.

## ACKNOWLEDGMENTS

This work has been partially supported by AFOSR under MURI Grant No. FA 9550-04-1-0359, NSF under Grant No. ECCS-0347502, OSC under Grants No. PAS-0061 and No. PAS-0110, and SBC endowment to The Ohio State University.

[1] A. Figotin and I. Vitebsky, Phys. Rev. E **63**, 066609 (2001).
[2] A. Figotin and I. Vitebskiy, Phys. Rev. B **67**, 165210 (2003).
[3] A. Figotin and I. Vitebskiy, Phys. Rev. E **68**, 036609 (2003).
[4] A. Figotin and I. Vitebskiy, J. Magn. Magn. Mater. **300**, 117 (2006).
[5] A. Figotin and I. Vitebskiy, Waves Random Complex Media **16**, 293 (2006).
[6] K.-Y. Jung, B. Donderici, and F. L. Teixeira, Phys. Rev. B **74**, 165207 (2006).
[7] H. X. Da, J. C. Wu, and Z. Y. Li, Appl. Phys. Lett. **91**, 172515 (2007).
[8] A. Figotin and I. Vitebskiy, Phys. Rev. E **72**, 036619 (2005).
[9] K.-Y. Jung, F. L. Teixeira, and R. Lee, IEEE Antennas Wireless Propag. Lett. **6**, 643 (2007).
[10] K.-Y. Jung and F. L. Teixeira, Phys. Rev. B **77**, 125108 (2008).
[11] A. Figotin and I. Vitebskiy, Phys. Rev. A **76**, 053839 (2007).
[12] E. Yablonovitch, Phys. Rev. Lett. **58**, 2059 (1987).
[13] J. D. Joannopoulos, R. D. Meade, and J. N. Winn, *Photonic Crystals: Molding the Flow of Light* (Princeton University Press, Princeton, NJ, 1995).
[14] G. Mumcu, K. Sertel, and J. L. Volakis, IEEE Antennas Wireless Propag. Lett. **5**, 168 (2006).
[15] A. Yariv and P. YEH, *Photonics: Optical Electronics in Modern Communications*, 6th ed. (Oxford University Press, New York, 2007).
[16] J. L. Volakis, G. Mumcu, and K. Sertel, IEICE Trans. Commun. **E90-B**, 2203 (2007).
[17] R. A. Chilton, K.-Y. Jung, R. Lee, and F. L. Teixeira, IEEE Trans. Microwave Theory Tech. **55**, 2631 (2007).
[18] A. A. Chabanov, Phys. Rev. A **77**, 033811 (2008).
[19] H. Rao, R. Scarmozzino, and R. M. Osgood, Jr., IEEE Photon. Technol. Lett. **14**, 477 (2002).
[20] S. Ju, K.-Y. Jung, and H. Kim, IEEE Antennas Wireless Propag. Lett. **13**, 414 (2003).
[21] Such a change in $\phi_{A2}$ is not the sole route to achieve a dispersion curve with SBE since the latter is determined by a combination of geometrical and materials parameters.
[22] On the other hand, an increase in $\phi_{A2}$ makes the dispersion relation develop a RBE.